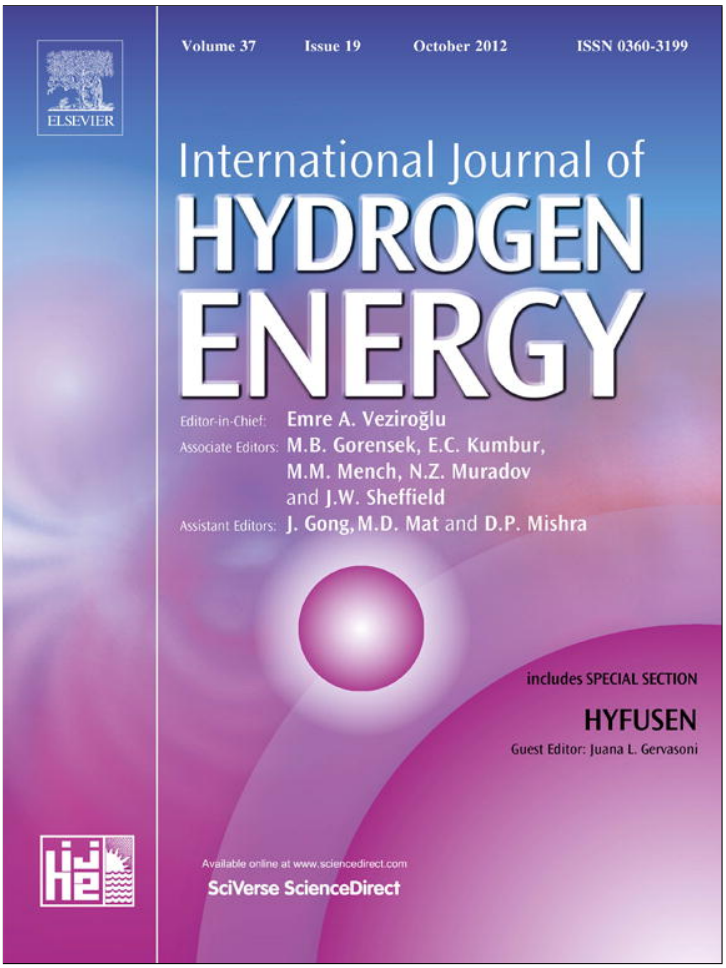

INTERNATIONAL JOURNAL OF HYDROGEN ENERGY 37 (2012) 14887–14894

Available online at www.sciencedirect.com

SciVerse ScienceDirect

journal homepage: www.elsevier.com/locate/he

Theoretical study of the ethanol steam reforming in a parallel channel reactor

Yanina M. Bruschi, Eduardo López, Noemí S. Schbib, Marisa N. Pedernera, Daniel O. Borio*

PLAPIQUI (UNS-CONICET), Camino La Carrindanga, Km. 7, 8000 Bahía Blanca, Argentina

ARTICLE INFO

Article history:
Received 26 August 2011
Received in revised form
29 December 2011
Accepted 31 January 2012
Available online 19 March 2012

Keywords:
Hydrogen production
Ethanol steam reforming
Heat transfer
Square channel
Pd catalyst

ABSTRACT

The ethanol steam reforming (ESR) is studied in a parallel plate reactor with square channels of 500–2000 μm and washcoated with Pd-based catalyst. The endothermic process is co- or countercurrently heated by means of a flue gas stream flowing through contiguous channels. Two contiguous square channels, assumed as representative of the whole reactor behavior, are simulated using both 1D pseudohomogeneous and heterogeneous models for comparison purposes. The influence of the main operating variables, flow configuration and design parameters on the performance of the reformer has been analyzed.

The reactor performance is mainly controlled by the heat supply from the flue gas to the process stream. For low inlet temperatures of the ethanol + water feed, the countercurrent flow configuration allows improved heat recuperation and the reactor shows a higher performance. Conversely, when the feed is pre-heated upstream the reactor, the cocurrent scheme appears preferable due to a more favorable axial profile of heat transferred. The channel width has a strong influence on the hydrogen production rate and the residual methane slips when cocurrent operation is selected. For the countercurrent scheme, a more robust design is achieved in terms of ethanol conversion and hydrogen yield for variations in the feed temperature. Moreover, the channel dimension losses influence provided enough small channels are considered. The heat conduction phenomenon through the solid metal wall was studied varying the wall thickness; diminished reactor performance for thicker walls was observed due to a drop in the heat duty.

1. Introduction

The production of bioethanol by fermentation of sugar cane, corn or other agricultural waste is an attractive alternative for the generation of hydrogen or synthesis gas, suitable for fuel cells or the production of chemicals. Bioethanol has high energy density and, due to its lower toxicity and volatility, is easier to store, handle and transport safely than other fuels. Some attention has been paid recently to processes for the production of H_2 or synthesis gas from bioethanol by means of catalytic ethanol steam reforming (ESR) [1–3].

Several mechanisms and kinetics have been proposed for the ESR using different catalysts. A number of kinetic models have been published for ESR using Ni, the most common

* *Corresponding author*.
E-mail address: ybruschi@plapiqui.edu.ar (Y.M. Bruschi).
0360-3199/$ – see front matter Copyright © 2012, Hydrogen Energy Publications, LLC. Published by Elsevier Ltd. All rights reserved.
doi:10.1016/j.ijhydene.2012.01.175

catalyst for steam reforming processes [4–6]. Other experimental and simulation studies also evaluated the use of Ni based catalysts for ESR [7–10].

Simson et al. [11] carried out a kinetic and experimental study for ESR using a Rh/Pt washcoated monolith catalyst. Other studies have analyzed the ESR process on Pt–Ni [12], Co/Al_2O_3 [13], Fe–Mn promoted Co/ZnO catalysts [14], Ce–Zr–Co oxide catalysts [15] and Ru catalysts [16].

López et al. [17] performed the kinetic modeling of ESR on a washcoated Pd-based catalyst. The authors considered three catalytic reactions: ethanol reforming, methane reforming and water gas shift reaction. ESR on Pd-based catalyst was also studied by Galvita et al. [18], Goula et al. [19], Scott et al. [20] and Hyman and Vohs [21].

Several types of reactors can be used for H_2 production, depending on the process scale, the operation constraints and the availability of raw materials. Tubular reformers are currently used in the industrial reforming of natural gas or heavier hydrocarbons. Other technologies, such as the Autothermal Reformers (ATR) can be used in large-scale plants as the methanol or Fisher-Tropsch synthesis [22].

Multichannel catalytic reactors have been suggested as an alternative to carry out methane steam reforming, a highly endothermic process [23]. Particularly, micro-/millireactors offer a high surface to volume ratio and high heat and mass transfer coefficients, which makes them appropriate for processes requiring high specific heat fluxes. Microreactors have recently received considerable attention in the literature [24–27].

Lab-scale micro-/millireactors can be electrically heated and isothermal conditions can usually be assumed because of their small geometry and high heat conductivity of materials [28]. However, for larger production scales, the heat supply should be provided through other sources, e.g., catalytic combustion in contiguous channels [23,29,30] or convective heating using flue gas coming from an external combustion chamber [23,31].

The present proposal takes this last option by considering a combustion chamber upstream the reactor. The heat generated in the chamber can be used not only to provide the reaction heat but also for former steps such as the evaporation and superheating of the feed stream (ethanol + water) up to the reaction temperature [9,32]. The ESR process can be improved by using ethanol as a fuel in order not to use additional fuels [9]. This work focuses on the non-isothermal behavior of both co- and countercurrently heated reformers of ethanol; the influence of the heat supply on hydrogen yield and methane generation is analyzed.

2. Mathematical model

A scheme of the reactor under analysis is shown in Fig. 1a [33]. As shown, adjacent foils with square channels are used to circulate the reactant mixture ($C_2H_5OH + H_2O$) and a flue gas stream coming from an external chamber, which supplies the heat required for the endothermic reforming reactions. Cocurrent and countercurrent flow configurations are adopted for the simulation as shown in Fig. 1b and c. A Pd-based

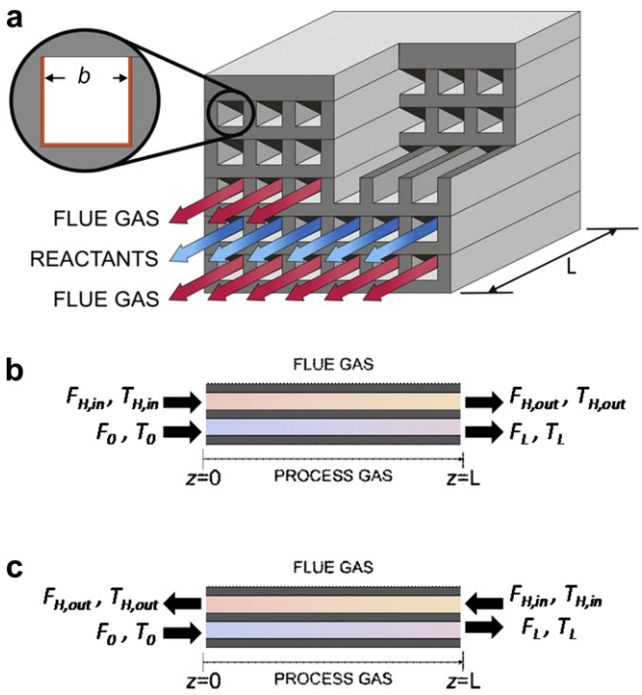

Fig. 1 – a) Schematic representation of the ESR reactor. Details of the flow configurations under study: b) Cocurrent, c) Countercurrent.

catalyst is assumed to be coated on the metallic microchannels. The following system of reactions is considered:

$$C_2H_5OH + H_2O \rightarrow CH_4 + CO_2 + 2H_2 \quad \Delta H_{R,1} = 8.73 \quad kJ/mol \tag{1}$$

$$CH_4 + H_2O \leftrightarrow CO + 3H_2 \quad \Delta H_{R,2} = 205.8 \quad kJ/mol \tag{2}$$

$$CO + H_2O \leftrightarrow CO_2 + H_2 \quad \Delta H_{R,3} = -41.17 \quad kJ/mol \tag{3}$$

Reaction (1) is assumed as irreversible, while reactions (2) and (3) are equilibrium-limited [17].

The microreactor is represented by means of a one dimensional heterogeneous model, subject to the following assumptions:

- Isobaric conditions: laminar flow through the channels without pellets ensures low pressure drops.
- Heat losses from the microreactor to the environment are neglected (the reactor is assumed to be perfectly isolated).
- Axial heat conduction through the solid wall is taken into account.
- Temperature and composition gradients in the cross section are not taken into account (the use of small channels supports the assumption of flat mass and temperature radial profiles).
- Uniform flowrate for all the microchannels, i.e., a proper flow distributor is assumed [25].
- Two contiguous channels (reactants and flue gas) are modeled as representative of the whole reactor.

The balance equations for the process, flue gas and solid phase are given below:

Process gas

$$\frac{dF_j}{dz} = A_T \sum_{i=1}^{3} (\upsilon_{j,i} r_i) \frac{A_{CAT}}{V_R} \tag{4}$$

$$\frac{dT}{dz} = \frac{A_T h a (T_S - T)}{\sum_{j=1}^{N} F_j C_{P,j}} \tag{5}$$

for j = Et, H_2O, CH_4, CO_2, CO, H_2

Flue gas

$$\frac{dT_H}{dz} = -\frac{A_{T,H} h_H a_H (T_H - T_S)}{\sum_{j=1}^{N_H} F_{j,H} C_{P,j}} \tag{6}$$

for j = H_2O, CO_2, O_2, N_2

Reactor wall

$$\frac{d^2T_S}{dz^2} = \frac{1}{keb}\left[2(b - wc)h(T_S - T) + 2(b - 2wc)h(T_S - T) - 4bh_H(T_H - T_S) + 3b\left(\sum_{i=1}^{3} r_i(T_S)\Delta H_{R,i}\right)\right] \tag{7}$$

for i = 1, 2, 3 (reactions (1)–(3))

Boundary conditions

Cocurrent

$$z = 0 \quad \begin{cases} F_j = F_{j,0} \\ T = T_0 \\ T_H = T_{H,in} \\ \dfrac{dT_S}{dz} = 0 \end{cases} \tag{8}$$

$$z = L \quad \left\{\frac{dT_S}{dz} = 0\right. \tag{9}$$

Countercurrent

$$z = 0 \quad \begin{cases} F_j = F_{j,0} \\ T = T_0 \\ \dfrac{dT_S}{dz} = 0 \end{cases} \tag{10}$$

$$z = L \quad \begin{cases} T_H = T_{H,in} \\ \dfrac{dT_S}{dz} = 0 \end{cases} \tag{11}$$

The symbols F_j and $F_{j,H}$ represent the molar flows of species j per *channel*, flowing on the process and flue gas sides, respectively.

The differential Equations (4)–(7) along with the boundary conditions (Eqs. (8)–(11)) were discretized using second order finite differences. The resultant algebraic system (600–1200 equations) was solved by means of a Broyden routine.

For comparison purposes, results arising from a pseudo-homogeneous model already reported by Anzola [33] are considered.

The operating conditions are shown in Table 1. A typical feed composition for ethanol steam reforming is assumed [6,16,28].

The power law kinetic expressions (r_1, r_2 and r_3) reported by López et al. [17] have been used in the simulations. The kinetic parameters for the Pd catalyst were obtained for a steam to carbon ratio in the range 2–4 and temperatures lower than 800 °C.

The heat transfer convective coefficients of each side were obtained from the Nusselt expression for square channel structured reactors proposed by Cybulski et al. [34].

The geometric parameters considered constant through the simulations here are L = 0.08 m (channel length) and wc = 1 μm (washcoat thickness) [28]. Similar washcoat thicknesses have been reported elsewhere [24,31]. A value of k = 18 W/mK for the stainless-steel conductivity was adopted from Outokumpu [35].

The present work includes the study of the influence of different values of the channel width (b = 500, 1000 and 2000 μm) on the reactor performance. Consequently, to keep constant the total cross sectional free area ($A_T \cdot NC$, see Table 2) we adjusted the total number of channels in each case, which is the same for the process and flue gas sides. In these terms, we achieved a constant value of the linear velocity of both flue gas and process streams (u and u_H, respectively, see Table 2).

3. Results and discussion

3.1. *Influence of the heat transfer resistances*

To account for the influence of the heat transfer resistances on both sides of the metallic wall, the results of the heterogeneous model presented in Section 2 are compared with those of a homogeneous model [33]. In this simplified version of the model, the energy balance for the metallic wall (Eq. (7)) is not considered and the reaction rates are evaluated at the temperature of the process gas. Fig. 2 shows the hydrogen yield as affected by the channel width (b), for the two flow configurations under analysis: countercurrent (Fig. 2a) and cocurrent (Fig. 2b). The results were obtained for a common

Table 1 – Operating conditions.

Feed pressure, P	0.1 MPa
Total molar feed flowrate, F_0	0.127 mol/s
Steam to carbon molar ratio, S/C	3
Total molar flue gas flowrate, F_H	0.18 mol/s
Flue gas molar fractions, %	
CO_2	10.43
H_2O	15.78
O_2	3.05
N_2	70.74
Inlet temperatures on the reaction side, T_0	100–900 °C
Inlet temperature on the flue gas side, $T_{H,in}$	900, 1000 °C

Table 2 – Constant parameter values for reactants and flue gas sides.

$A_T NC = 12.45\ cm^2$	Total cross sectional free area
$L = 0.08$ m	
$u = 7.41$ m/s	
$u_H = 12.9$ m/s	

flue gas inlet temperature ($T_{H,in} = 1000$ °C) and two values of the process gas inlet temperature ($T_0 = 100$ and 500 °C). The remaining operating conditions are kept constant. For each feed temperature, both models predict higher yields as the channel width decreases, due to the availability of higher heat transfer areas and heat transfer coefficients. However, the heterogeneous model predicts higher hydrogen yields than its homogeneous version, for all the studied operating conditions. As it can be seen, the differences in the predictions of both models become significant as the channel dimensions increase. For a channel width of 2000 μm, the differences in the calculated H_2 yields become as high as 84% for the countercurrent scheme with an inlet temperature of 100 °C. The reasons of these important deviations are the significant differences in the temperature of the solid and gas phases. In fact, the heterogeneous model evaluates the reaction rates at the temperature of the metallic wall, which is higher than that of the process gas at most of the axial positions (results not shown). Therefore, the homogeneous model leads to underestimations of the ethanol conversion and hydrogen yield. Similar results to those shown in Fig. 2 were obtained for other operating conditions and design parameters. Excepting reactor designs comprising channels with very small dimensions (e.g., $b < 200$ μm), the use of a heterogeneous model is necessary to achieve adequate quantitative results. Therefore, the upcoming results were obtained profiting the heterogeneous model.

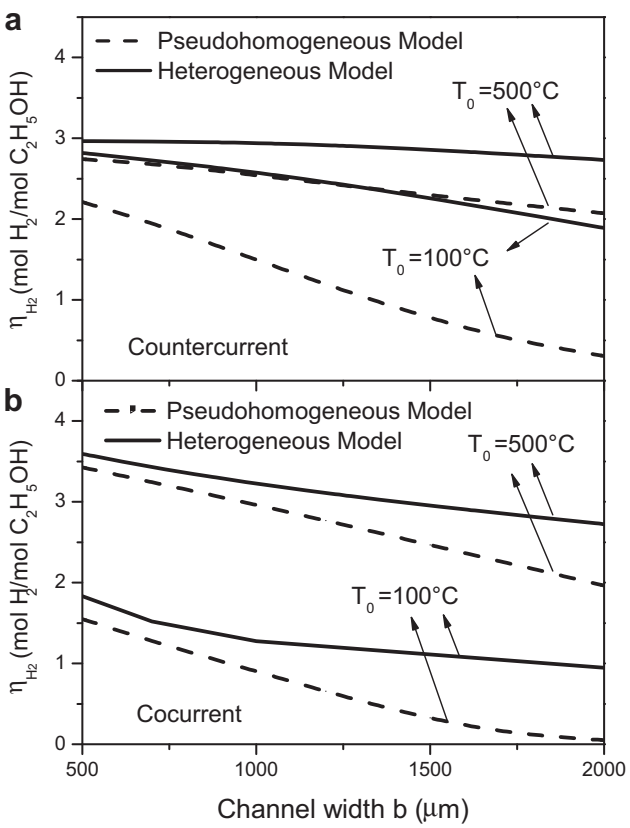

Fig. 2 – Hydrogen yield vs. channel width for two different flow configurations: a) Countercurrent, b) Cocurrent. $T_{H,in}$ = 1000 °C.

3.2. *Analysis of flow configuration*

Fig. 3 reports results concerning ethanol conversion (a) and hydrogen yield (b) for different values of the inlet temperature of the process gas and for two alternatives of flow configuration, namely, co- and countercurrent. As expected, both conversion and yield increase with the process gas inlet temperature (T_0) favoring not only higher ethanol conversions but also higher degrees of conversion of the intermediate methane, yielding extra hydrogen amounts. For relatively low T_0, (e.g., condition 1 in Fig. 3) the countercurrent scheme leads to higher performances as the feed stream can be more efficiently pre-heated inside the reactor up to the reaction temperature. Conversely, for operating conditions including the feeding to the reactor of and externally pre-heated stream (e.g., condition 2 in Fig. 3), the cocurrent configuration appears

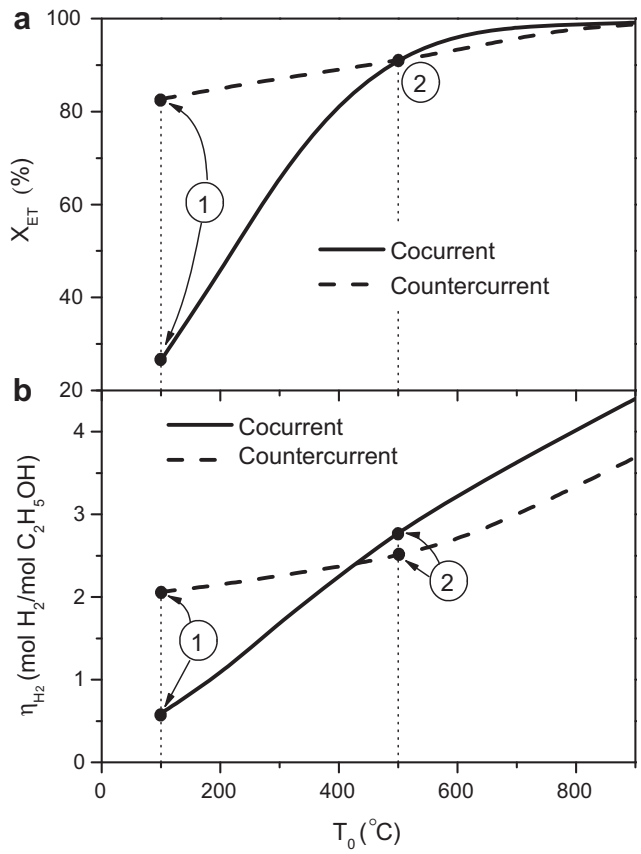

Fig. 3 – Influence of the inlet temperature of the feed stream on ethanol conversion (a) and hydrogen yield (b) for cocurrent and countercurrent schemes. $T_{H,in}$ = 900 °C, b = 1000 μm.

more convenient. To clarify this analysis, Fig. 4 shows axial temperature profiles of the flue gas (T_H), solid wall (T_S) and process stream (T) for both flow configurations for operating point 1 of Fig. 3. Similarly, Fig. 5 reports results corresponding to operating condition 2 of Fig. 3. Additionally, axial profiles of hydrogen yield for the operating conditions under analysis (in Figs. 4 and 5) are depicted in Fig. 6. When the reactor has to be used to preheat a cold inlet feed ($T_0 = 100$ °C), see Fig. 4, the cocurrent scheme shows a rather isotherm solid temperature at ca. 520 °C. However, this temperature level is low to achieve a significant degree of ethanol conversion; in fact only 28% X_{ET} is achieved (see operating point 1 of Fig. 3a). Conversely, a countercurrent flow configuration allows the operation in the last fourth of the reactor at solid temperature levels higher than 580 °C, with a final value $T_S = 735$ °C. The axial T profiles are highly non-isothermal and, at least, the first half of the reactor is used as a simple heat exchanger to preheat the incoming cold feed. As shown in Fig. 6, hydrogen yields are negligible for the countercurrent scheme (for $T_0 = 100$ °C) at $z < 0.04$ m and significant levels are only reported toward the reactor outlet. Accompanying the rather flat solid temperature profile shown for the cocurrent configuration at low inlet temperature (Fig. 4), Fig. 6 reports an axial hydrogen generation in the whole reactor length but at poor rates.

Operating conditions including an already (externally) preheated feed (e.g., $T_0 = 500$ °C, see Fig. 5), cocurrent operation leads to a mean solid temperature significantly higher than in the previous case ($T_0 = 100$ °C) and an appreciably decreasing behavior of temperature profile. This higher temperature level makes possible the achievement of higher ethanol conversion and hydrogen yield (see Fig. 3). Interestingly, beyond $z = 0.02$ m the axial T profile of the process stream surpasses T_S, becoming this last one the coldest temperature of the three up to the reactor end. Under these conditions, the solid phase receives heat from both process and flue gas streams and acts as a heat sink due to the endothermal reactions. The countercurrent scheme (Fig. 5) shows qualitatively similar temperature profiles as those of Fig. 4, increasing with the reactor length. However, the total temperature increase of the solid is lower, $\Delta T_S = 241$ K, when compared with the 573 K observed in Fig. 4. As explained for cocurrent flow, higher mean temperature levels conduct to higher conversions and hydrogen yields. If the feed temperature were increased under countercurrent flow at values surpassing 550–600 °C, a minimum in the solid temperature could occur at some intermediate coordinate of the reactor.

Comparing the inlet-outlet temperature differences of the flue gas stream, it can be concluded that the countercurrent configuration leads to higher heat duties. In fact, the total heat

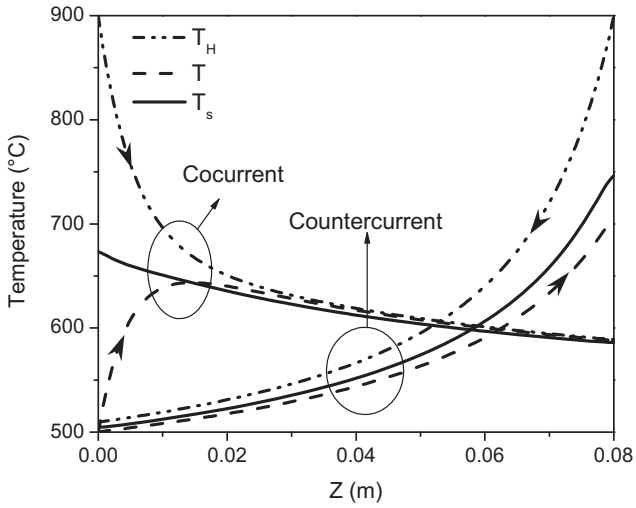

Fig. 5 – Axial profiles of temperature corresponding to the operating condition 2 of Fig. 3 for cocurrent and countercurrent schemes. $T_0 = 500$ °C.

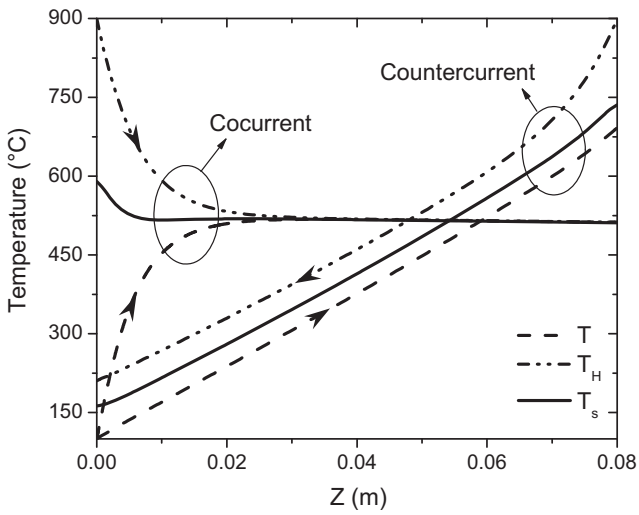

Fig. 4 – Axial profiles of temperature corresponding to the operating condition 1 of Fig. 3 for cocurrent and countercurrent scheme. $T_0 = 100$ °C.

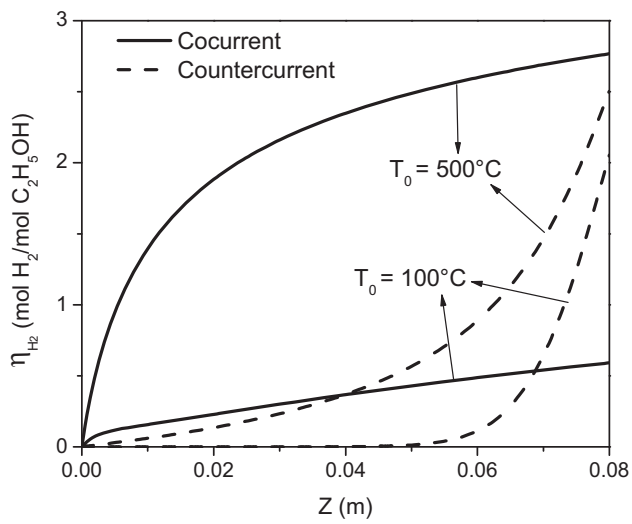

Fig. 6 – Axial profile of hydrogen yield for the same operating conditions as Figs. 4 and 5.

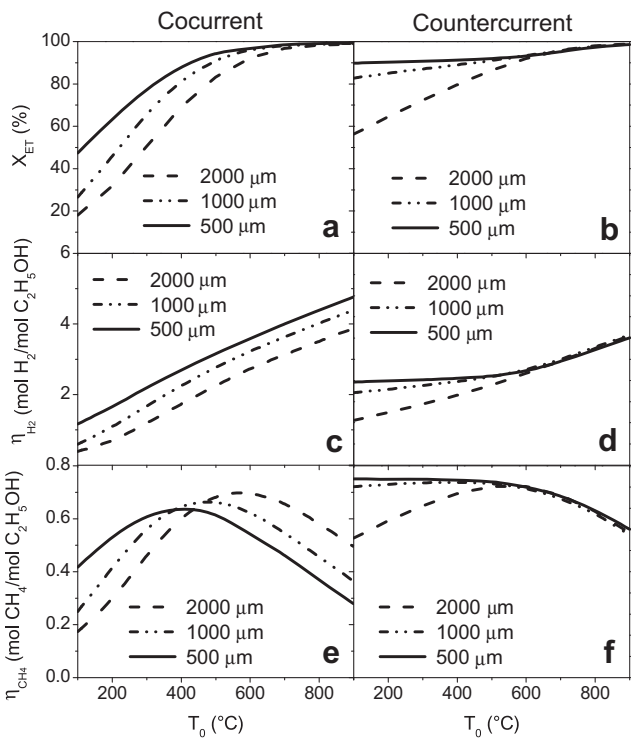

Fig. 7 – Influence of T_0 on ethanol conversion, hydrogen and methane yield for three different channel widths. $T_{H,in}$ = 900 °C.

supply, i.e., $Q_T = F_H\ C_{pH}\ (T_{H,in} - T_{H,out})$ is higher for the countercurrent scheme for the operating conditions of both Figs. 4 and 5. However, the hydrogen yield shows a more complex behavior. As referenced elsewhere [33,36], an axially decreasing heat flux profile is favorable for steam reforming reactions. This corresponds to the case of a cocurrent configuration. As a result, when the feed stream is pre-heated enough upstream the reactor (e.g., Fig. 5), a cocurrent scheme should be selected [33]. Conversely, if the feed needs to be pre-heated inside the reactor (Fig. 4), a countercurrent configuration results the best option.

3.3. *Influence of the geometrical parameters*

The influence of the channel width (b) and the inlet temperature (T_0) on the reformer performance is shown in Fig. 7, for both flow configurations.

As smaller channels are selected, the heat transfer area per unit volume as well as the heat transfer coefficients increase considerably. For a same value of the feed temperature, the heat transferred from the flue gas to the process side increases as b diminishes. In terms of reactor performances, consequently, ethanol conversions and hydrogen yields improve. As seen in Fig. 7b, for low T_0 and channel width values the ethanol conversion is relatively high and scarcely sensitive with respect to the feed temperature for countercurrent scheme. Similar trends are observed for the hydrogen and methane yield in Fig. 7d and f, respectively. As shown in Figs. 4 and 6, under these conditions the countercurrent reactor is acting in the first section as a feed preheater. If the selected b values are smaller enough, the available heat exchange area is overdesigned for the process requirements, and the outlet yields are relatively insensitive with respect to the feed temperature.

For low T_0 values and cocurrent flow, conversely, the ethanol conversion (Fig. 7a) is strongly dependent on both T_0 and b. The hydrogen and methane yields (Fig. 7c and e, respectively) present a similar behavior to the ethanol conversion. This fact is consistent with the reaction scheme being considered, where the ethanol is decomposed in both methane and hydrogen (reaction (1)).

At high feed temperatures, the ethanol conversion is almost complete in all the cases, particularly for the cocurrent case. As stated before, the hydrogen yield at high T_0 values is higher for the cocurrent scheme at the different channel widths under consideration (Fig. 7c and d). At almost complete ethanol conversion, the hydrogen yield increases continuously with T_0 due to further methane steam reforming (see Fig. 7e). The cocurrent scheme is still dependent on the selected channel width, being the countercurrent configuration practically insensitive with respect to the value of b.

3.4. *Axial heat transport through the solid wall*

Table 3 reports results concerning the effect of the heat transport through the metallic walls of the channels; higher wall thickness means a wider path for heat to be axially spread. Disregarding the selection of a co- or a countercurrent flow configuration, higher wall thickness leads to higher isothermicity of the axial profiles of the solid wall temperature (lower ΔT_S) and to diminished heat duties. These lower heat duties, consequently, lead to lower ethanol conversions and lower hydrogen yields. These results qualitatively accord with those reported elsewhere [37,38].

Table 3 – Influence of the wall thickness (e) on hydrogen yield.

	Cocurrent			Countercurrent		
e (μm)	1000	2000	3000	1000	2000	3000
ΔT_s (K)	74.73	62.24	54.49	396.74	363.92	340.61
X_{ET} (%)	40.14	39.33	38.78	75.10	71.99	69.49
η_{H_2} molH_2/molC_2H_5OH)	0.914	0.893	0.879	1.796	1.705	1.6343
Duty (kW)	0.488	0.407	0.356	2.587	2.372	2.2212

4. Conclusions

The effect of the design parameters on the performance of an ethanol steam reformer has been analyzed for different schemes of flow for the process and flue gas streams, namely, co and countercurrent configurations.

A comparison of the results provided by using either a pseudohomogeneous or a heterogeneous model of the reactor points that the use of the last one becomes mandatory to achieve accurate results of the reactor performance for almost all the design configurations selected here (i.e., channel widths and flow scheme).

The simulation results demonstrate that the hydrogen yields are mainly controlled by the heat supply from the flue gas to the process stream. For low inlet temperatures of the ethanol + water feed, the countercurrent flow configuration allows improved heat recuperation and the reactor shows a higher performance. Conversely, when the feed is preheated upstream the reactor, the cocurrent scheme appears preferable due to a more favorable axial heat transferred axial profile. The channel width (b) has a strong influence on the hydrogen production rate and the residual methane slips when cocurrent operation is selected. A more robust design is achieved for countercurrent flow, in terms of ethanol conversion and hydrogen yield for variations in the feed temperature. Moreover, the channel dimension losses influence provided enough small channels are considered. The heat conduction phenomenon through the solid metal wall was studied varying the wall thickness; diminished reactor performance for thicker walls was observed due to a drop in the heat duty.

Acknowledgments

Support to this work through Universidad Nacional del Sur (UNS) and Consejo Nacional de Investigaciones Científicas y Tecnológicas (CONICET) is gratefully acknowledged.

Notation

a	heat transfer area per unit volume $2bL/(b^2L)$, m^2/m^3
A_{CAT}	catalyst area, m^2
A_T	cross sectional area of channels b^2, m^2
b	width of square channel, μm
$C_{p,j}$	specific heat of component j, J/(mol K)
e	fin width, μm
F	molar flow (mol/s)
h	heat transfer coefficient, $W/(m^2\ K)$
$\Delta H_{R,i}$	heat of reaction of reaction i, J/mol
k	wall thermal conductivity, W/(m K)
L	channel length, mm
NC	number of channels
N	number of components
P	total pressure (both sides), MPa
Q	total heat flux, kW
r_i	reaction rate of reaction i, i=1,2,3, $mol/(m^2_{cat}\ s)$
S/C	Steam to carbon molar ratio, $molH_2O/molC$
T	temperature (reaction side), °C
T_s	wall temperature, °C
T_H	temperature (flue gas side), °C
u	average velocity, m/s
V_R	volume of reaction channel, m^3
wc	thickness of the washcoated catalyst, μm
X_{ET}	ethanol conversion, dimensionless
z	axial coordinate, m

Greek letters

η_i	yield of component i, dimensionless
$\upsilon_{j,i}$	stoichiometric coefficient of component j for reaction i, dimensionless

Subscripts

cat	catalyst
Et	ethanol
H	heating gas (flue gas)
i	reaction i
j	component j
L	at the axial coordinate $z = L$
0	at the axial coordinate $z = 0$
in	inlet
out	outlet

REFERENCES

[1] Haryanto A, Fernando S, Murali N, Adhikari S. Current status of hydrogen production techniques by steam reforming of ethanol: a review. Energy and Fuels 2005;19:2098–106.

[2] Vaidya PD, Rodrigues AE. Insight into steam reforming of ethanol to produce hydrogen for fuel cells. Chemical Engineering Journal 2006a;117:39–49.

[3] Ni M, Leung DYC, Leung MKH. A review on reforming bio-ethanol for hydrogen production. International Journal of Hydrogen Energy 2007;32:3238–47.

[4] Akande A, Aboudheir A, Idem R, Dalai A. Kinetic modeling of hydrogen production by the catalytic reforming of crude ethanol over a co-precipitated Ni-Al_2O_3 catalyst in a packed bed tubular reactor. International Journal of Hydrogen Energy 2006;31:1707–15.

[5] Mas V, Baronetti G, Amadeo N, Laborde M. Ethanol steam reforming using Ni(II)-Al(III) layered double hydroxide as catalyst precursor. Kinetic study. Chemical Engineering Journal 2008a;138:602–7.

[6] Mas V, Bergamini ML, Baronetti G, Amadeo N, Laborde M. A kinetic study of ethanol steam reforming using a nickel based catalyst. Topics in Catalysis 2008b;51:39–48.

[7] Aboudheir A, Akande A, Idem R, Dalai A. Experimental studies and comprehensive reactor modeling of hydrogen production by the catalytic reforming of crude ethanol in a packed bed tubular reactor over a Ni/Al_2O_3 catalyst. International Journal of Hydrogen Energy 2006;31:752–61.

[8] Akpan E, Akande A, Aboudheir A, Ibrahim H, Idem R. Experimental, kinetic and 2-D reactor modeling for simulation of the production of hydrogen by the catalytic reforming of concentrated crude ethanol (CRCCE) over a Ni-based commercial catalyst in a packed-bed tubular reactor. Chemical Engineering Science 2007;62:3112–26.

[9] Arteaga LE, Peralta LM, Kafarov V, Casas Y, Gonzales E. Bioethanol steam reforming for ecological syngas and

electricity production using a fuel cell SOFC system. Chemical Engineering Journal 2008;136:256–66.
[10] Denis A, Grzegorczyk W, Gac W, Machocki A. Steam reforming of ethanol over Ni/support catalysts for generation of hydrogen for fuel cell applications. Catalysis Today 2008;137:453–9.
[11] Simson A, Waterman E, Farrauto R, Castaldi M. Kinetic and process study for ethanol reforming using a Rh/Pt washcoated monolith catalyst. Applied Catalysis B: Environmental 2009;89:58–64.
[12] Soyal-BaltacIoglu F, Aksoylu AE, Önsan ZI. Steam reforming of ethanol over Pt-Ni catalysts. Catalysis Today 2008;138: 183–6.
[13] Sahoo DR, Vajpai S, Patel S, Pant KK. Kinetic modeling of steam reforming of ethanol for the production of hydrogen over Co/Al_2O_3 catalyst. Chemical Engineering Journal 2007; 125:139–47.
[14] Torres JA, Llorca J, Casanovas A, Domínguez M, Salvadó J, Montané D. Steam reforming of ethanol at moderate temperature: multifactorial design analysis of Ni/La_2O_3-Al_2O_3, and Fe- and Mn-promoted Co/ZnO catalysts. Journal of Power Sources 2007;169:158–66.
[15] Vargas JC, Libs S, Roger A-C, Kiennemann A. Study of Ce-Zr-Co fluorite-type oxide as catalysts for hydrogen production by steam reforming of bioethanol. Catalysis Today 2005; 107–108:417–25.
[16] Vaidya PD, Rodrigues AE. Kinetics of steam reforming of ethanol over a Ru/Al_2O_3 catalyst. Industrial and Engineering Chemistry Research 2006b;45:6614–8.
[17] López E, Gepert V, Gritsch A, Nieken U, Eigenberger G. Ethanol steam reformingin a parallel-plate reactor with coupling of exothemic and endothermic reactions, in press.
[18] Galvita VV, Semin GL, Belyaev VD, Semikolenov VA, Tsiakaras P, Sobyanin VA. Synthesis gas production by steam reforming of ethanol. Applied Catalysis A: General 2001;220: 123–7.
[19] Goula MA, Kontou SK, Tsiakaras PE. Hydrogen production by ethanol steam reforming over a commercial Pd/γ-Al_2O_3 catalyst. Applied Catalysis B: Environmental 2004;49:135–44.
[20] Scott M, Goeffroy M, Chiu W, Blackford MA, Idriss H. Hydrogen production from ethanol over Rh-Pd/CeO_2 catalysts. Topics in Catalysis 2008;51:13–21.
[21] Hyman MP, Vohs JM. 2009. An investigation of the interaction between catalyst and support in Pd/ZnO and Co/ZnO catalyzed alcohol decomposition. 2009 AIChE Annual Meeting, 09AIChE. Nashville, TN.
[22] Joensen F, Rostrup-Nielsen JR. Conversion of hydrocarbons and alcohols for fuel cells. Journal of Power Sources 2002;105: 195–201.
[23] Frauhammer J, Eigenberger G, Hippel LV, Arntz D. A new reactor concept for endothermic high-temperature reactions. Chemical Engineering Science 1999;54:3661–70.
[24] Ehrfeld W, Hessel S, Löwe H. Microreactors, new technology for modern chemistry. Mainz: Wyley–Vch; 2000.
[25] Hessel V, Hardt S, Löwe H. Chemical micro process engineering. Fundamentals, modelling and reactions. Weinheim: Wyley-Vch; 2004.
[26] Karakaya M, Avci AK. Comparison of compact reformer configurations for on-board fuel processing. International Journal of Hydrogen Energy 2010;35:2305–16.
[27] López E, Irigoyen A, Trifonov T, Rodríguez A, Llorca J. A million-channel reformer on a fingertip: Moving down the scale in hydrogen production. International Journal of Hydrogen Energy 2010;35:3472–9.
[28] Görke O, Pfeifer P, Schubert K. Kinetic study of ethanol reforming in a microreactor. Applied Catalysis A: General 2009;360:232–41.
[29] Casanovas A, Saint-Gerons M, Griffon F, Llorca J. Autothermal generation of hydrogen from ethanol in a microreactor. International Journal of Hydrogen Energy 2008;33:1827–33.
[30] Arzamendi G, Diéguez PM, Montes M, Centeno MA, Odriozola JA, Gandía LM. Integration of methanol steam reforming and combustion in a microchannel reactor for H_2 production: a CFD simulation study. Catalysis Today 2009; 143:25–31.
[31] Cai W, Wang F, van Veen A, Descorme C, Schuurman Y, Shen W, et al. Hydrogen production from ethanol steam reforming in a micro-channel reactor. International Journal of Hydrogen Energy 2010;35:1152–9.
[32] Giunta P, Mosquera C, Amadeo N, Laborde M. Simulation of a hydrogen production and purification system for a PEM fuel-cell using bioethanol as raw material. Journal of Power Sources 2007;164:336–43.
[33] Anzola AM, Bruschi YM, López E, Schbib NS, Pedernera MN, Borio. Heat supply and hydrogen yield in an ethanol microreformer. Industrial and Engineering Chemistry Research 2011;50:2698–705.
[34] Cybulski A, Stankiewicz A, Edvinsson Albers RK, Moulijn JA. Monolithic reactors for fine chemicals industries: a comparative analysis of a monolithic reactor and a mechanically agitated slurry reactor. Chemical Engineering Science 1999;54:2351–8.
[35] Outokumpu, editor. Steel grades, properties and global standards. Sweden: Outokumpu Stainless, Avesta Research Centre; 2004.
[36] Piña J, Schbib NS, Bucalá V, Borio DO. Influence of the heat-flux profiles on the operation of primary steam reformers. Industrial and Engineering Chemistry Research 2001;40: 5215–21.
[37] Andisheh Tadbir M, Akbari MH. Methanol steam reforming in a planar wash coated microreactor integrated with a micro-combustor. International Journal of Hydrogen Energy 2011;36:12822–32.
[38] Kolios G, Glöckler B, Gritsch A, Morillo A, Eigenberger G. Heat-integrated reactor concepts for hydrogen production by methane steam reforming. Fuel Cells 2005;5(1):52–65.